

PHYS 396 - Project Report

Daniela Breitman (260792446)

McGill University Department of Physics

May 4, 2019

Abstract

When a signal hits the steel mesh of the CHIME radio telescope, it starts as a mere voltage and ends as an event in a database. During this journey, there are many random processes which somewhat distort the signal. We know these processes can be mitigated, which is why we are trying to understand how the sensitivity of the telescope varies over time. To measure it, we need to rely on known cosmic sources to act as calibrators. Since CHIME is a transit telescope, why not just use the sky to calibrate? This research project demonstrated that, in fact, there exist three reliable sources whose daily measurements indeed seem to reflect the daily sensitivity of the telescope. Pulsars B2217+47, B1508+55, and B1946+35 appear very stable in their pulse count over time, but a plot of their mean SNR unveils many interesting variations that most likely reflect the variation in the sensitivity of the telescope. We also find that simply tracking the pulse counts of the top 10 most observed pulsars also gives a good idea of the sensitivity. Lastly, we discuss some sources that have peculiar patterns in their data that hint at scintillation.

Contents

1	Introduction	1
1.1	Radio Astronomy	1
1.2	Radio Pulsars	2
1.3	Fast Radio Bursts	3
1.4	CHIME	4
1.5	Instrument Calibration	6
1.5.1	Gain Fluctuation	7
2	Methods	7
2.1	Big Picture	8
2.2	Pulsar Selection	9
2.3	Data Visualization	9
3	Results	10
3.1	Big Picture	10
3.2	Single Source	12
3.2.1	Stable Sources	12
3.2.2	Grouped Behaviour	13
3.3	Other Results of Interest	13
4	Discussion	14
4.1	Many Source Analysis	14
4.2	Single Source Analysis	15
5	Conclusion	16
A	Appendix	18
A.1	Calculations	18
A.2	Additional Figures	19
A.3	Other Results of Interest	23

1 Introduction

For almost a century did physicists expect to detect radio waves from outer space. Ever since Maxwell wrote his equations, there were multiple attempts to detect astronomical radio waves. However, due to technical limitations, all of them were unfruitful. It was only in 1932 that electrical engineer Karl Jansky detected the very first radio astronomical waves from the center of our Milky Way [1]. As often in science, Jansky discovered it by pure chance. Indeed, it is a series of such serendipitous discoveries that painted the way for modern radio astronomy.

1.1 Radio Astronomy

The radio band is extremely wide, even *too* wide, for it to make sense to consider a single telescope design to see it all, which is why there exist many radio telescope designs. Each has a specific mission. In spite of the variety in ground-based telescope design, there are many general patterns: as large a collecting area as possible, a magnifying subreflector, and mobility to point it to different patches of the sky. The large collecting area helps the telescope detect faint objects. The magnifying subreflector is a tiny dish placed above the main dish to let signals bounce off the main dish twice and thus magnify them. The mobility of the telescope allows observers to look at different places at the sky. Rapidly shifting between beams (aka Dicke switching [2]) also helps get rid of noise. However, a realistic single-dish telescope can only do so much in terms of angular resolution and pointing accuracy. The key to overcoming this limitation is interferometry: we synchronize many dishes together, thus increasing the effective area and the angular resolution of the telescope. Arrays of telescopes also help decrease noise and amplify signals detected by more than one dish using aperture synthesis. This technique gave us a new outlook on the sky from ground-based telescopes, not to mention all the new discoveries it brought. [2]

1.2 Radio Pulsars

The early 20th century drew an exponential curve in our knowledge of the atom. Shortly after the discovery of the neutron, physicists Walter Baade and Fritz Zwicky proposed the revolutionary idea of a star made up of neutrons as an aftermath of a supernova. For many years, the concept of neutron stars was not developed. Until, when chance came, and Anthony Hewish and Jocelyn Bell detected the first radio pulsar. [3]

Radio pulsars are currently known to be highly magnetized, rapidly rotating neutron stars with heavily misaligned rotation and magnetic axes. The pulsar emits radiation beams from the magnetic poles, and as it rotates, much like a lighthouse. Well placed observers have the luck to measure those beams as a series of pulses. Thus, as the radio beam from B1919+21 - the first pulsar to be discovered - shines on Earth, astronomers observe a radio 'blip' that corresponds to a single rotation of the pulsar. Sometimes, when the magnetic and rotation axes are nearly orthogonal, beams from both poles can be observed so that two pulses correspond to a single pulsar rotation.

Pulsars are believed to emit in the entire electromagnetic spectrum, but we usually only see them in the radio band. [3] Today, over 2300 pulsars are known, with periods ranging from about 1.4ms to about 8s . The majority of the pulsar population is confined to the Galactic Plane, but is still very incomplete.

When radio pulses are emitted far away in space, the pulse is deformed by the time it reaches Earth. More specifically, the observed pulse is dispersed because lower frequencies move through a plasma of electrons more slowly than higher frequencies. For an observer at a distance d from the source, the dispersion delay time t is thus: [2]

$$t = \left(\frac{e^2}{2\pi m_e c} \right) \nu^{-2} \int_0^d n_e dl \quad (1)$$

We then define the dispersion measure (DM) as the integrated free electron density along the line of sight from an observer to a source with separation d :

$$DM \equiv \int_0^d n_e dl$$

The DM is the number necessary to correct the dispersed parabolic signal back to a sharp pulse (notice the ν^{-2} dependence in (1)). Thus, as a general rule, the farther away the object is, the more free electrons we expect to be on its path and the higher is its DM. [2]

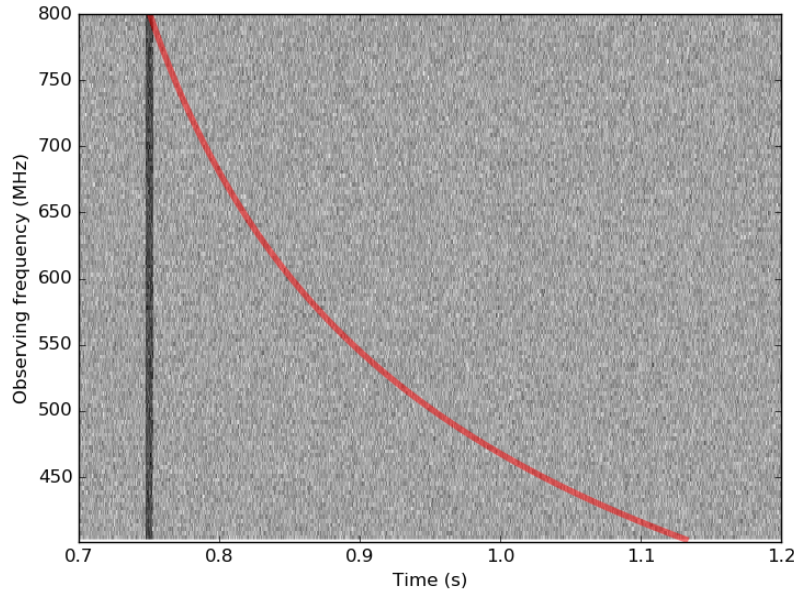


Figure 1: A dispersed ($DM = 20 \text{ pc} \cdot \text{cm}^{-3}$) pulse with peak SNR of 50 and pulse width of 5 ms in red. Notice the parabolic shape due to the ν^{-2} dependence in frequency as expected from the dispersion time delay equation above. In gray, a dedispersed pulse (equivalent to $DM = 0 \text{ pc} \cdot \text{cm}^{-3}$). Both pulses are computer generated. Courtesy of Emilie Parent.

1.3 Fast Radio Bursts

Fast forward to 2007, when a bright short burst was discovered by Lorimer and Narkevic while going through pulsar data from the Parkes Telescope. The burst had many characteristics different from pulsars. For starters, the burst was very dispersed, meaning its origin was probably extragalactic in contrast to pulsars. And obviously, the burst was unique - it was not repeating. Today, these short extragalactic bursts with a high dispersion measure (DM) are known as fast radio bursts (FRBs). The Lorimer burst, for example, had a DM of 375 pc cm^{-3} in comparison with the 75 pc cm^{-3} predicted by NE2001 - a model for Galactic electron density distribution. Soon after, other teams from the Parkes Telescope discovered FRBs and later, other telescopes began seeing them too. Over 30 of them are published to

date and yet their physical origin is still unknown. To add to the mystery, some FRBs are also known to repeat, however irregularly. Although common radio telescopes discovered the first few FRBs, they were not designed to do it. [4] It is the Canadian Hydrogen Mapping Experiment (CHIME), although designed for cosmology, that is today the leader in FRB discovery with over 300 single-pulsed FRBs and several repeaters.

1.4 CHIME

The Canadian Hydrogen Intensity Mapping Experiment (CHIME) is a novel transit radio telescope that saw first light in September 2017. Many of its design choices were motivated by the main experiment it hosts which is the Hydrogen intensity mapping of the northern sky to measure the expansion of the Universe. In particular, it is sensitive in the 400 MHz – 800 MHz frequency range - a very interesting range to be looking at since the early population of FRBs had higher frequencies, and thus is an excellent instrument to search for FRBs in an unexplored frequency range.



Figure 2: CHIME telescope, seen at night from the northwest. Image credit to CHIME Collaboration.

CHIME has no moving parts. It sees the exact same sky every day. It is the sum of 4 20m x 100m cylindrical paraboloidal reflector dishes conveniently aligned North-South which

yields a collecting area of 8000 m². That comes down to a field of view of about 200 square degrees of sky at any given time, while most telescopes can see only a few degrees. Above each cylinder hang 256 equally spaced dual polarization feeds for a total input of 2048 signals into the two East and West receiver huts where the CHIME correlator amplifies and splits the inputs into 1024 frequency channels. From the steel mesh cylinders, the data enters the CHIME correlator which is made up of the F-Engine and the X-Engine. The former channelizes and digitizes the inputs, and the latter correlates the signals in space. [4]

The F-Engine digitizes 13.1 Tb/s of data from the 2048 signal inputs. A filter bank then breaks up each of the 2048 inputs of 400 MHz into 1024 bins of 390 kHz. The data is further condensed and is then passed on to the X-Engine to be spatially correlated. The X-Engine is built of 256 processing computer nodes where the data undergoes the first of 5 data processing stages, called L0. L0 is responsible for performing a Fast Fourier Transform algorithm to generate 256 formed beams along the N-S direction. Four beams are formed along the E-W direction, to yield a total of 1024 discrete beams whose exact spacing can be tuned as needed. It is also at this stage that gain offset is applied to every frequency channel. The gains are calculated daily by monitoring a very bright source like Cyg A, and are used to correct for all kinds of small variations in the system such as the length of the cables from the cylinders to the receiver huts. [4]

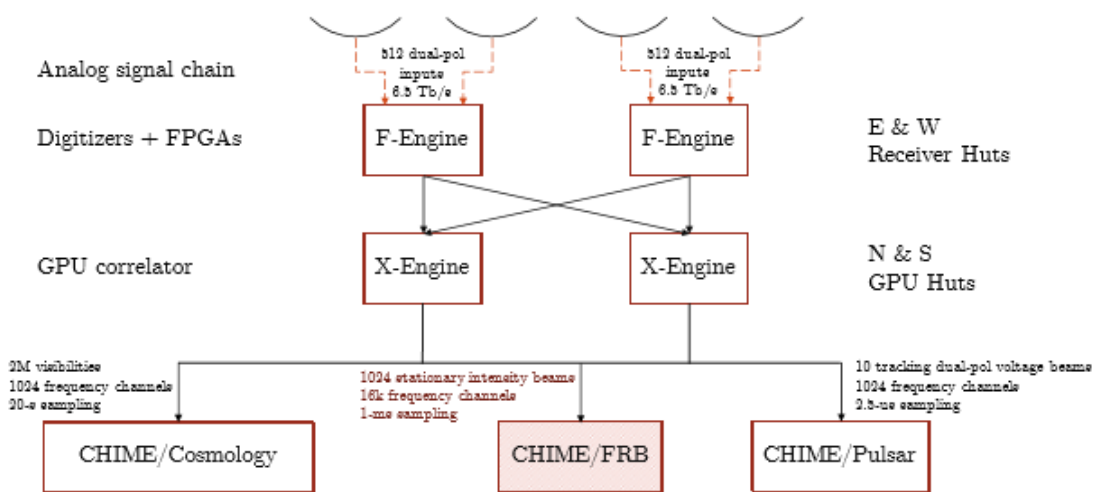


Figure 3: Diagram of the CHIME telescope signal path, starting from the four cylinders (four black arcs) to the F and X Engines, all the way to the CHIME/FRB huts [4].

From L0, the data is sent to the CHIME/FRB processing CPUs where stages L1-L4 occur. In L1, signals deemed as noise are rejected, and the remaining pulses are dedispersed (see 1.2). Their DM is calculated by finding the best fit parabola with a DM range of up to $13\,000 \text{ pc cm}^{-3}$ for a pulse width of up to 128ms. An algorithm called *bonsai* calculates the signal-to-noise ratio of the pulses in addition to searching for high SNR pulses with DM trials in real time. In L2, an algorithm decides whether a single event is composed of more than one detection, as brighter pulses may be detected in multiple beams and have different DMs assigned to them. The main criterion for this decision, among others, is that the beams of the detection should be neighbours and classified as a group. In L3, the data is filtered further to flag extragalactic events which are of interest. The data is compared to a database consisting of the well-known ATNF pulsar catalogue, an FRB catalogue and an RRAT catalogue. Events are also classified by a decision tree which determines what should be done with every kind of event. L4 applies those actions e.g call to L1 for more detailed data, or alert everyone for an event of interest, and saves the data. [4]

1.5 Instrument Calibration

The CHIME software pipeline is composed of many complex algorithms and since calibration is applied very early on in X-Engine, the efficiency of the telescope is very dependent on the quality of that calibration. Calibrating CHIME is quite a challenge - how can we calibrate a telescope that doesn't move i.e without pointing it at a specific source? As a start, we want to build a tool that would allow us to track the daily health of the telescope, to see how various changes in the pipeline affect it, in addition to random processes. We do so by looking at the data flagged as a known source (i.e pulsars) and track daily statistics on it. Albeit simple, this analysis provides insightful information on the status of the telescope. To maximize FRB detection and better understand our data, it's crucial for us to know how well the CHIME system performs on any given day. We want to tie this measure of performance to our daily instrument calibration i.e gain update as well.

1.5.1 Gain Fluctuation

The focal line of the CHIME telescope, in addition to containing the feeds, also houses low-noise amplifiers that multiply weak signals to milliwatt levels. This amplified signal is then sent to the receiver huts. In the receiver hut, the 1024 inputs are further amplified and digitized. The output voltage of the receiver is proportional to its power gain G . The issue is that if G isn't absolutely constant, its fluctuation generates a false signal which is indistinguishable from noise. Thus, gain fluctuation will reduce the sensitivity of the telescope unless it is corrected for by, for example, comparing the signals in adjacent feeds. [2] [4] Gain fluctuations are a random process so the sensitivity of the telescope changes slightly every day. To keep the telescope at optimal sensitivity, we need to reduce these fluctuations as much as possible. However, it is not always easy to see how they affect the data since they mutate all frequency inputs randomly.

Currently, there is no formula to know which phase shifts are better than others. For now, we just look at the signal-to-noise ratio (SNR) and calibrate our instrument with a bright source like Tau-A or Cyg-A. The calculated gains, applied in the X-Engine, generate a phase shift in the signals we measure which usually result in an overall improvement in sensitivity. However there is no optimal recipe yet.

The goal of this project is, consequently, to monitor data from known sources to quantify the daily performance of the telescope, and relate it to daily gain updates to shed some light on finding an ultimate metric to quantify the daily telescope health.

2 Methods

I focused on two distinct methods to monitor the telescope health: first, by looking at a large amount of pulsar data at once, and second, by looking at a small number of hand-picked pulsars daily. The data I use is from the last big chunk of stable running time, that is from mid-November 2018 to early March 2019.

2.1 Big Picture

The first step is to query the database. The event selection is tailored for each event as we want the most statistically relevant data. Obviously, we query events flagged as known sources with SNR greater than or equal to 8, but we also calculate the transit time of the known source and only consider events within 15 minutes of the transit time. Knowing the position of the source from the catalogue, we can also predict the beam number where the source should be detected at a given time with our current beam model. Moreover, we take the beam position and their widths into account. The maximum N-S distance an event can have from

Partial	Off
18/11/19	18/12/03
18/12/06	18/12/04
19/01/28	18/12/05
19/01/29	18/12/07
	18/12/10
	18/12/11

Table 1: The dates are in format (yy/mm/dd).

the beam center is 0.5 degrees and 10' for E-W. From this large data set, we only consider the sources with the highest average pulse count over that period to eliminate statistical flukes. This also eliminates sources that we only saw a few with a few pulses, which we don't want in our analysis anyway. We want the most stable and reliable data possible. This is done by simply sorting the data by highest mean first and plotting from the top down e.g top 5 would grab the 5 most observed pulsars. Many plots can be made but the most useful ones are plots of number of detected pulses per day over the average number per source plotted over

time, and a histogram binning the observed number of pulses.

In the time span considered, there were 10 days when the telescope was either completely shut down or partially shut down (See Table 1). Although exposure isn't tracked in detail, a quick parse through a wide sample of data in right ascension (RA) allows us to see whether the telescope was off on a given day. To eliminate this source of bias, I decided to disregard the data for these days for all the sources, to make sure we consider only full working days. This way, every time the number of pulses observed for a given source for a given day is 0, then it is most likely that we didn't see that source for some reason other than the telescope being entirely off. It was also thus decided to include the zeros in the calculation of the means and standard deviations, since now we know for sure that a 0 pulse count means we didn't see a source, not that the telescope was off.

Moreover, we choose to exclude sources whose maximal number of pulses observed on a given day is under 4 as it is not significant enough.

The histogram is made with the normalized data of all the pulsars.

2.2 Pulsar Selection

When choosing specific pulsars to calibrate on, we consider two approaches. Either we make sure that they are as stable as possible, or we choose sources that appear to vary together as a group regardless of their stability. This is so that changes in the measurements imply changes in the system and not changes in the pulsar. We therefore look to filter out pulsars on many features such as giant pulses, nulling, and pulse magnification. For this purpose, we average the pulse per day count over time for all working days, and we pick the sources with the smallest standard deviation. For these sources, we are interested in the histogram counting the normalized number of pulses observed per day and their day-to-day behaviour. We may also look at the daily mean SNR of a source over time. The daily mean SNR of a source is calculated by taking the mean of every brightest pulse from every single event on that day and dividing it by the square of its time error/16 (See Appendix A for code snippet).

2.3 Data Visualization

To visualize this awesome amount of information, I built a highly interactive Bokeh viewer. The viewer reads the data files generated by the database query. The goal of the viewer is to allow fellow CHIME users to quickly be able to see the overall trends in the data, play with it, and compare to the daily data.

The viewer is quite complex in its operations at this point in its development since it offers many different features for the user. For example, it allows one to plot the data for as many sources as desired and change the parameters for the axes. It also offers a tab with the catalogue data to be able to quickly compare with data. There are many different filters available for the catalogue data plot, for example, one could filter for a specific DM range, or for sources that were observed by CHIME at some point. The axes and colour chart are also

customizable. The Bokeh platform allows users to navigate through the plots with all kinds of tools such as Zoom and Pan. Users can also save the plot as an image once they achieve their desired result. On the other hand, the histograms are generated via simple matplotlib plots since interaction isn't necessary.

3 Results

3.1 Big Picture

We choose to analyze the brightest sources as they are the most statistically relevant. We plot the top 5 and top 10 sources with highest average pulse count only as plotting more than 10 results in a mass of dots, without anything of interest being visible. We also plot a histogram of the normalized data of all the sources. A histogram of the same plot for the 5 and 10 sources with highest average pulse count can be found in Appendix A.

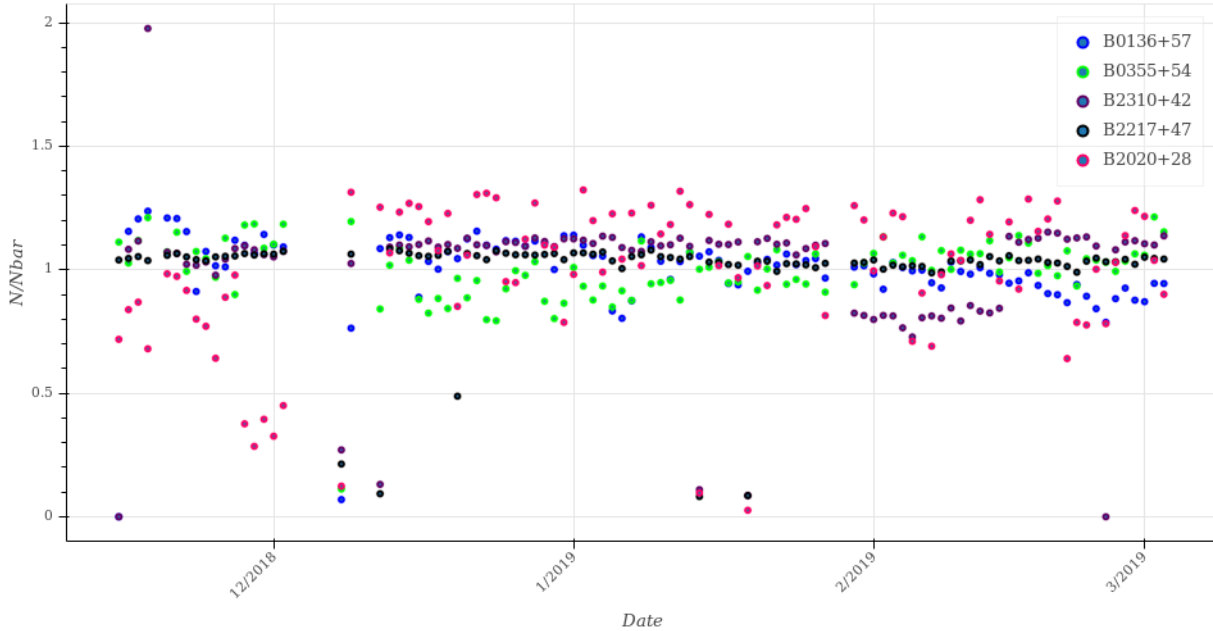


Figure 4: We plot the pulse count per day over the average count for the 5 sources with highest average pulse count over time, where the legend lists them in descending order of brightness. Their mean pulse counts are 1307, 1130, 975, 805 and 757 respectively. A version of this plot with error bars is included in Appendix A.

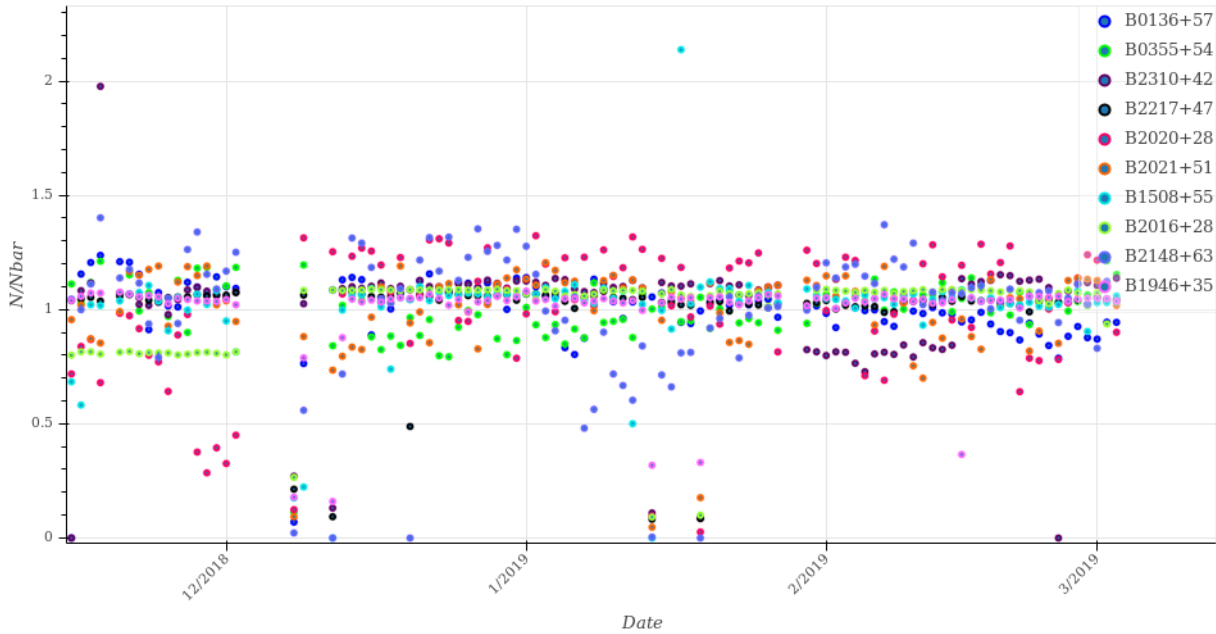


Figure 5: A plot of the pulse count per day over the average count for the 10 sources with highest average pulse count over time, where the legend lists them in descending order of brightness. Their mean pulse counts are 1307, 1130, 975, 805, 757, 742, 649, 599, 497, and 487 respectively. A version of this plot with error bars is available in Appendix A.

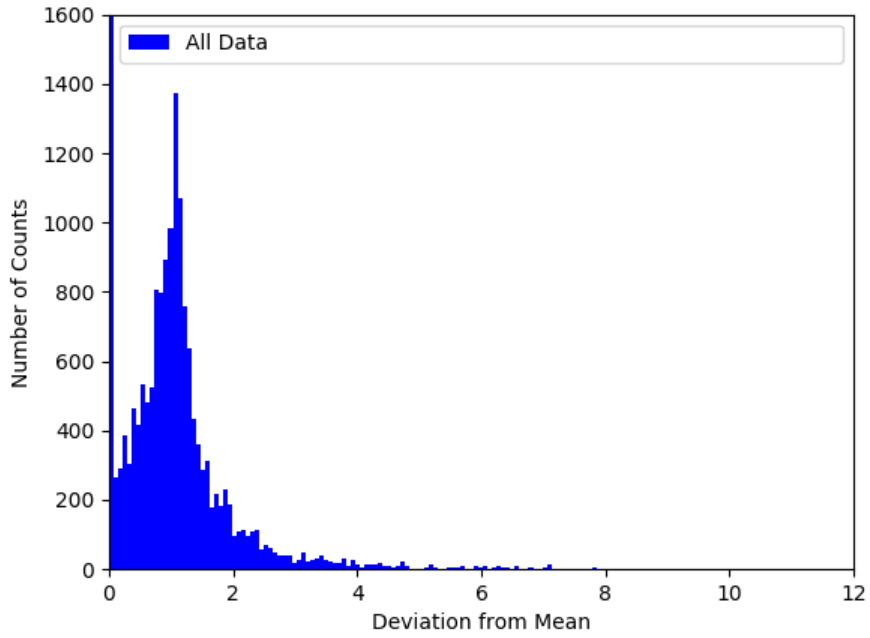


Figure 6: A histogram of all the normalized data of all 193 sources. The tail at 0 is cropped here and in fact extends all the way up to about 4000 counts, as there are many faint and irregular sources that are not seen at all on many days. See Appendix A for a histogram for the top 5 and top 10 sources with highest average pulse count.

3.2 Single Source

3.2.1 Stable Sources

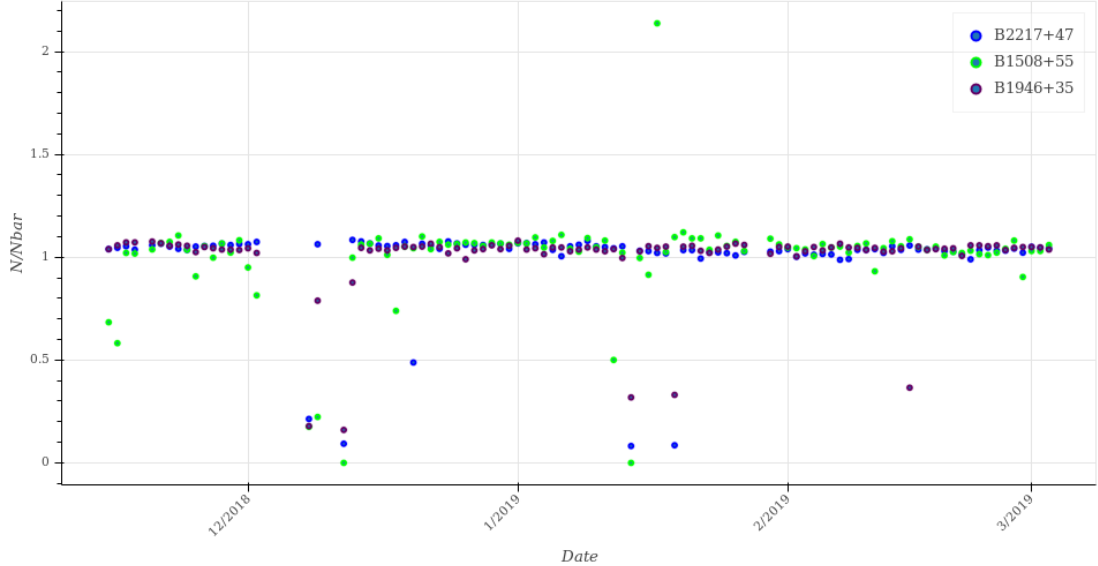


Figure 7: The pulse count per day over the mean pulse count of the three most stable sources plotted over time. In spite of a few outliers, the three are very concentrated around the mean. The same plot with error bars can be found in Appendix A.

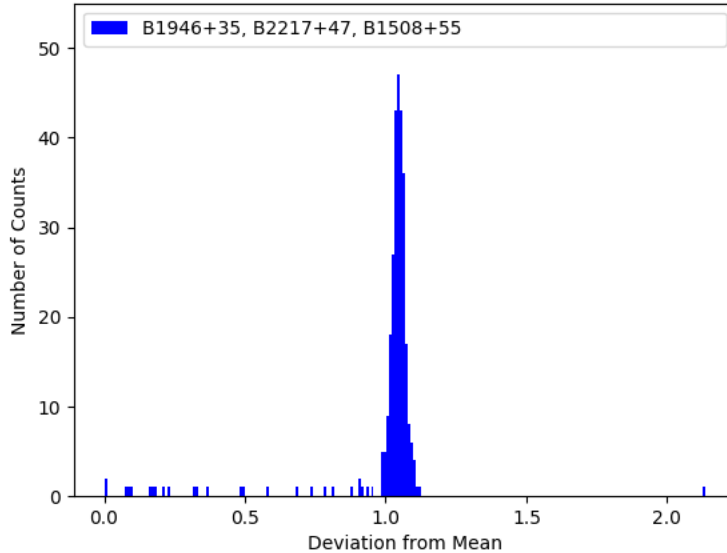


Figure 8: Histogram of all the data from the three most stable sources. We can see the data peak very sharply at the 1.0 mark as expected. The histogram for each source separately can be found in Appendix A. features are not present in high frequencies.

After examining each source individually, the sources that seem most stable are B2217+47, which also happens to be ranked with the second highest mean pulse count, B1508+55, and B1946+35. Since in Figure 7, the sources appear very stable, we also decide to include the plot of the mean SNR for this time period in hopes that we would see more patterns and variation. We note that B2217+47 is known for low-frequency pulse profile variation [5], however it seems that these

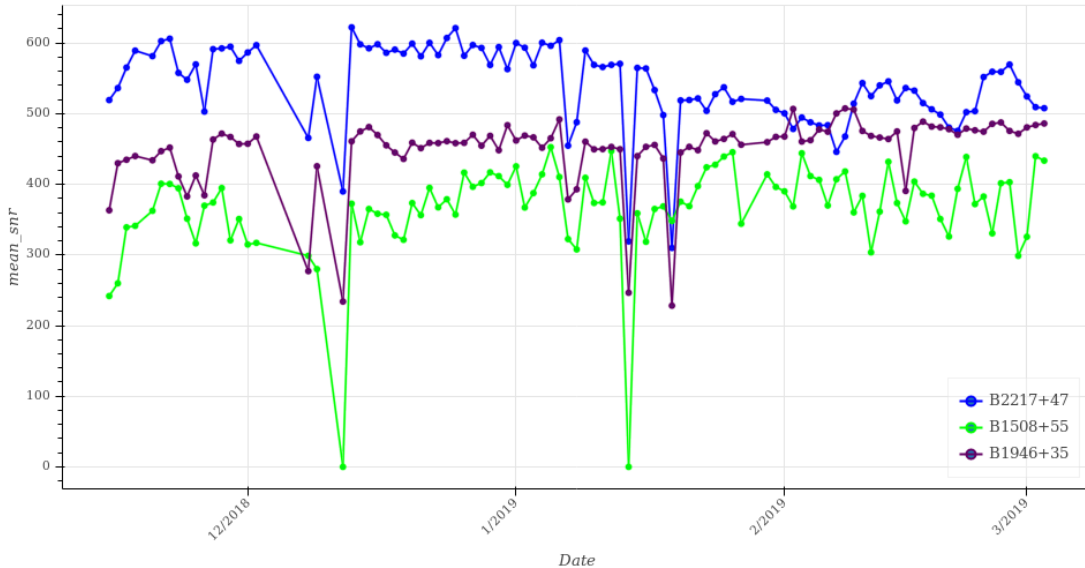


Figure 9: In contrast to Figure 7, here we see many more patterns. The calculation of the mean SNR plotted here can be found in Appendix A

3.2.2 Grouped Behaviour

It turns out that there are other sources whose mean SNR plot have the same trends as the ones seen in Figure 9. However, when plotting many of them at once, only the most pronounced effects are highlighted. The more intrinsic features are destroyed by the differences in each source. Thus, it might be an interesting continuation to the project to investigate this further such that it might yield results worth showing.

3.3 Other Results of Interest

While looking at the data for single source analysis, there were many sources that exhibited curious patterns. We were able to classify them into 5 main groups: step-like, spiky, ascending, descending, and wave-like. We show a plot for each category in Section 3.3 of Appendix A, where the results are discussed a bit in their captions.

4 Discussion

4.1 Many Source Analysis

In Figure 4, we see that the top 5 sources with the highest pulse count fluctuate a lot over time, except for B2217+47 that is also one of the stable sources considered in the single source analysis. In both Figures 4 and 5, we can see that there were 4 days, namely 18/12/08, 18/12/12, 19/01/14, and 19/01/19 (in (yy/mm/dd) format), where many of the pulsars seem to have behaved suboptimally. This is very unlikely to be a statistical coincidence and so we can safely say, that on a day of suboptimal performance, we'd observe **two or more of the top 10 sources with $N/\bar{N} < 0.8$.**

It is also very important to investigate what happened on 18/12/02 as we note a step-like jump in the data of B2016+28. Otherwise its data is also very stable. As mentioned in Section 3.3, there are other sources that exhibit this behaviour. The steps in the other two sources do happen to coincide (See Figure 16 in Appendix A). It is tricky to explain this phenomenon. The two sources whose step does coincide are very nearby in RA and Dec. Although one might think it might be caused by some issue with the computer nodes e.g a crash, the known source viewer (See 2.3) contradicts that explanation, as they are not predicted to be observed in nearby beams nor at the same time (about 3 hours and 6 beams apart). Other than that, these sources appear very stable and should be added the meagre list of 3 stable sources if this issue can be resolved internally and is not an intrinsic property of these pulsars.

In Figure 4, as well as in 7, we can see how very stable B2217+47 is. Thus, perhaps with a larger data sample, simply **the mean of the pulse count of B2217+47 and its two other stable counterparts** will be enough to tell how the telescope is performing on a given day. The main message from Figure 6 seems to be that unfortunately we're much more often under the average than above average, as the slopes of the curve on each side of the peak indicate. This plot would be useful to keep track of and see, in the long run, whether it becomes more symmetric or not. Moreover, it suggests that good sources to track would be those whose distribution is already symmetric at this stage, thus every day the data is

on the low side, the odds are it's the telescope that's at fault. For example, in Figure 8, we see that the histogram is already a bit asymmetric in favour of the low side. This suggests that only tracking those three might flag the bad days, but maybe not the suboptimal days. However if we look at Figure 13, the histogram of the top 10 pulsars (available in Appendix A), we notice that the distribution there is much more symmetric at the base of the peak, hinting that it might be a better sample. Figure 14, the histogram of the top 20 pulsars, is even more symmetric! We would then want **an algorithm to tell us whether we're on the left or on the right of the peak on any given day**.

Of course, since the top sources overall exhibit a more gaussian behaviour over time, the histogram over all sources is expected to be more symmetric for them. It is the faint and irregular sources that often happen to fall in the spiky category (See 3.3) that are responsible for this asymmetry and the tails in the plot: the pulse count remains at 0 for days at a time to the quickly rise to many times the average only to fall back down (See Figure 17). We also note that the peaks of the spiky sources do not coincide and thus do not seem to globally characterize telescope performance.

It is also worth mentioning that while the data of over 20 sources appears spiky, the data of others appears to rise or drop over the entire time period considered (See Figure 18 for more comments). Since in spite of their overall drop/rise, we still see the data coinciding for most of the time, this suggests that instead of looking for stable sources, it might be more indicative to look for **sources that display the same day to day pattern**. They might be the ones that will indeed characterize the efficiency of the telescope best.

4.2 Single Source Analysis

Using the three most stable sources as seen in Figure 7 seems to easily highlight the extremes i.e the 4 very suboptimal days mentioned earlier. However, they don't do a very good job at unveiling day to day patterns in their pulse count because they are so very stable. However, when plotting their mean SNR (calculation in Appendix A), we do notice many more patterns. Thus, although only drastic problems/improvements in the system would disrupt those perfect pulse count lines, their mean SNRs are much more sensitive to daily changes.

A change consistently visible in at least two of the three sources could imply

a change in the system. This analysis is probably the most robust and reliable up to now, since it relies on two levels of information, the pulse count and the mean SNR, but also because the information comes from very bright and stable sources. In fact, they rank 3rd, 6th, and 9th, respectively for mean pulse count, meaning their data is statistically very robust.

Although this project is already well under way, there are many aspects of it that can be easily improved if only there was more time. For example, taking daily operation hours into account isn't particularly challenging given there are members of the team tracking our daily up and down time. This will allow us to consider partial working days in our data set instead of just excluding it as we do now. Although it might be harder to implement, we should also take exposure into account. Fact is we see some sources for more time than other, thus it is obvious we'd get better SNR and higher pulse counts. Notice that for the three stable sources we chose, the declinations are of 47° , 55° , and 35° , all well-placed in the center of our declination range. Ideally we'd want to calibrate with sources over the entire declination range. These improvements suggested also bring forward some of the possible causes of error in this analysis. Another cause of error is the size of the data, 99 full days, which is somewhat limited for a long term analysis. A data set double the size would allow us to make much stronger claims.

5 Conclusion

In this project, we found out that there are three particularly bright sources, B2217+47, B1508+55, and B1946+35, that appear very stable. Although their normalized pulse count profiles don't seem to demonstrate any pattern other than obvious trends visible in most sources, their mean SNR, on the other hand, spills many secrets. The three sources truly seem to agree on multiple SNR drops and rises, much more than any other group of sources, allowing us to say that if at least two of them follow some pattern, then it must be indicative of the telescope performance. Moreover, we also show that tracking the sources in the top 10 pulse count also gives a good indication of the overall performance. Thus, the combination of these two tests ought to give a very good indication of the daily performance of CHIME FRB. Last but not

least, we note that there are many sources that exhibit very interesting pulse count profiles and/or SNR profiles over the given time period, often a sign of scintillation or giant pulses. Indeed, we find that some of the ones mentioned are already in the literature, but there are many that are not documented, leaving lots of room for very rich science.

References

- [1] W. T. Sullivan, *Cosmic Noise: A History of Early Radio Astronomy*. Cambridge University Press, 2009. [1](#)
- [2] J. J. Condon and S. M. Ransom, *Essential Radio Astronomy*. Princeton University Press, 2016. [1](#), [2](#), [3](#), [7](#)
- [3] V. Kaspi and M. Kramer, “Radio pulsars: The neutron star population fundamental physics,” in *arXiv:1602.07738*, 2016. [2](#)
- [4] CHIME Collaboration, “The chime fast radio burst project: System overview,” in *arXiv:1803.11235*, 2018. [4](#), [5](#), [6](#), [7](#)
- [5] D. Michilli et al., “Low-frequency pulse profile variation in psr b2217+47: evidence for echoes from the interstellar medium,” in *arXiv:1802.03473*, 2018. [12](#)
- [6] P.F. Wang et al., “Jiamusi pulsar observations: Ii. scintillations of 10 pulsars,” in *arXiv:1808.06406*, vol. 618, 2018. [25](#)

A Appendix

A.1 Calculations

```
for i in range(days):
    for j in range(len(events)):
        best = events[j].l1_events[np.argmax(events[j].l1_events['snr'])]
        :
        snrs.append(best['snr'] / np.sqrt(best['time_error'] / 16))
        :
results[i]['mean_snr'] = np.mean(snrs)
```

The error δ for each data point are calculated in the following way:

$$\delta = \frac{\sqrt{N}}{N} \quad (2)$$

A.2 Additional Figures

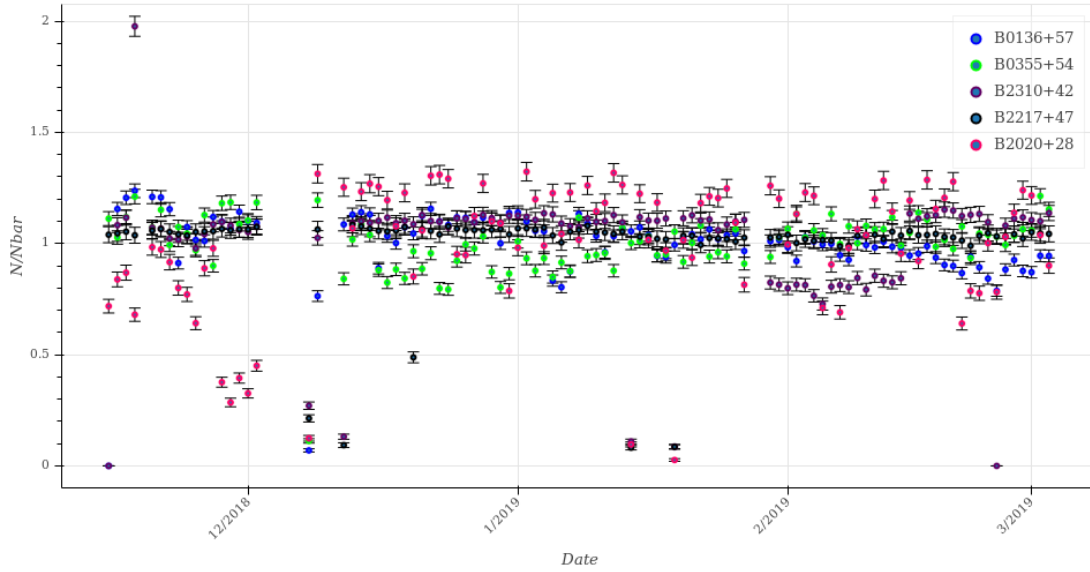


Figure 10: The pulse count per day over the mean pulse count of the 5 sources with highest average pulse count plotted over time. They are shown in descending order in the legend.

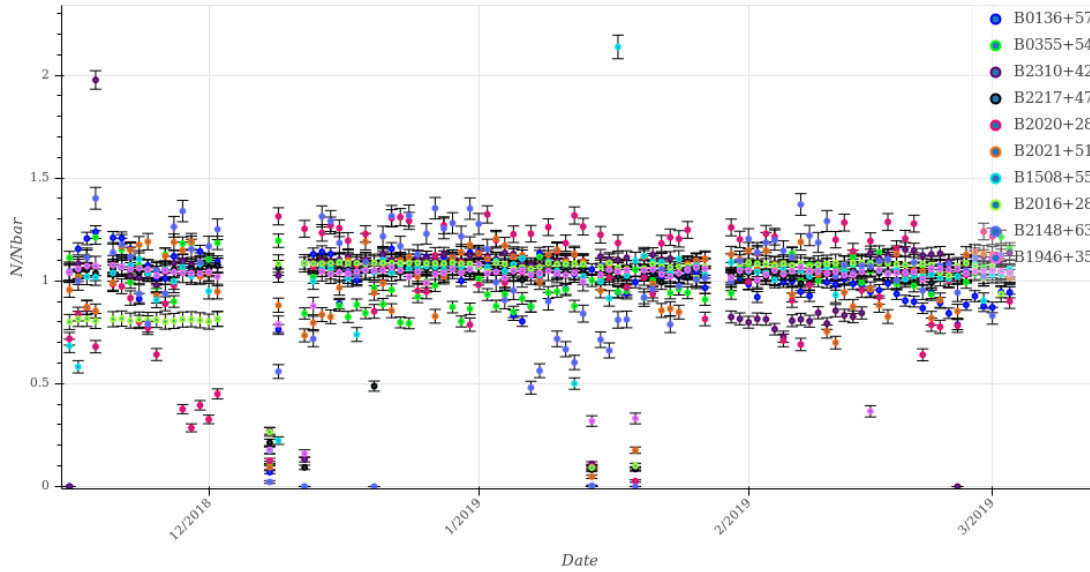


Figure 11: The pulse count per day over the mean pulse count of the 10 sources with highest average pulse count plotted over time. They are shown in descending order in the legend.

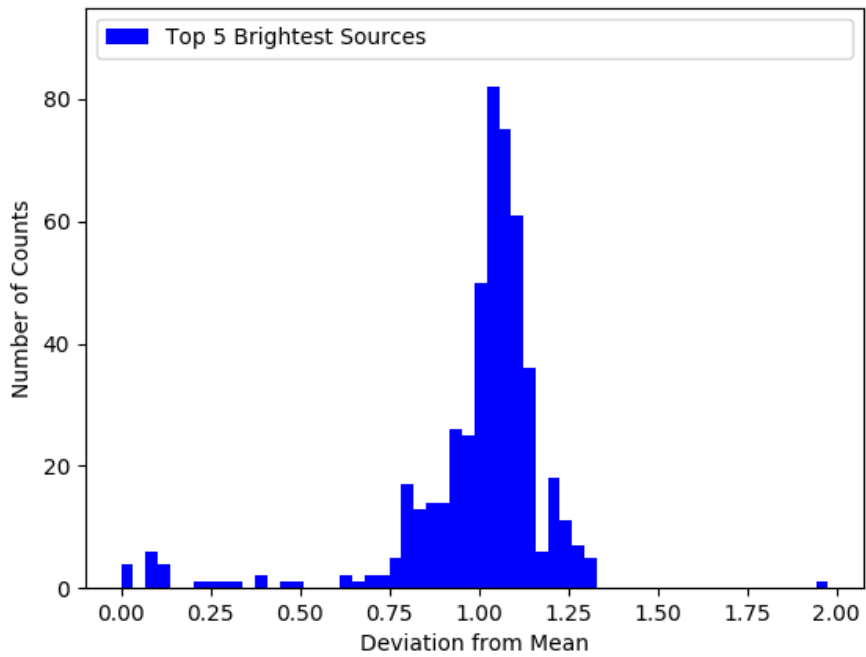


Figure 12: The histogram of all the normalized pulse counts for the 5 sources with highest average pulse count.

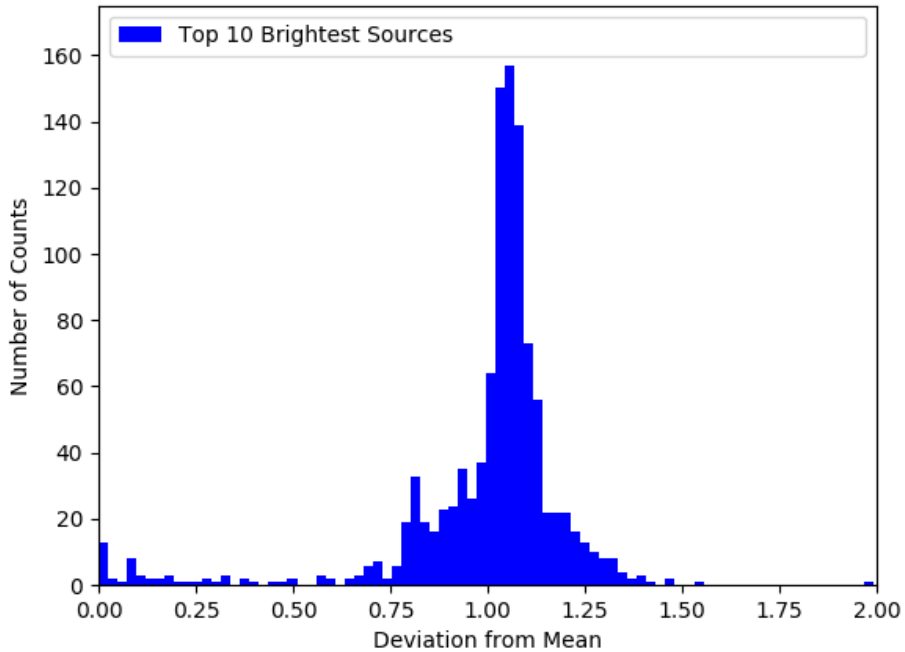


Figure 13: The histogram of all the normalized pulse counts for the 10 sources with highest average pulse count.

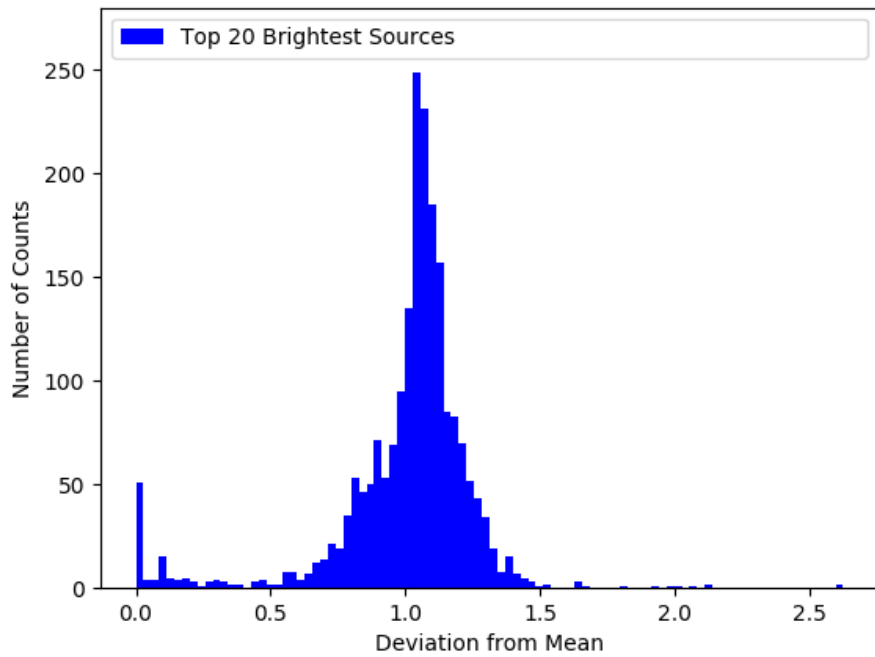


Figure 14: The histogram of all the normalized pulse counts for the 20 sources with highest average pulse count.

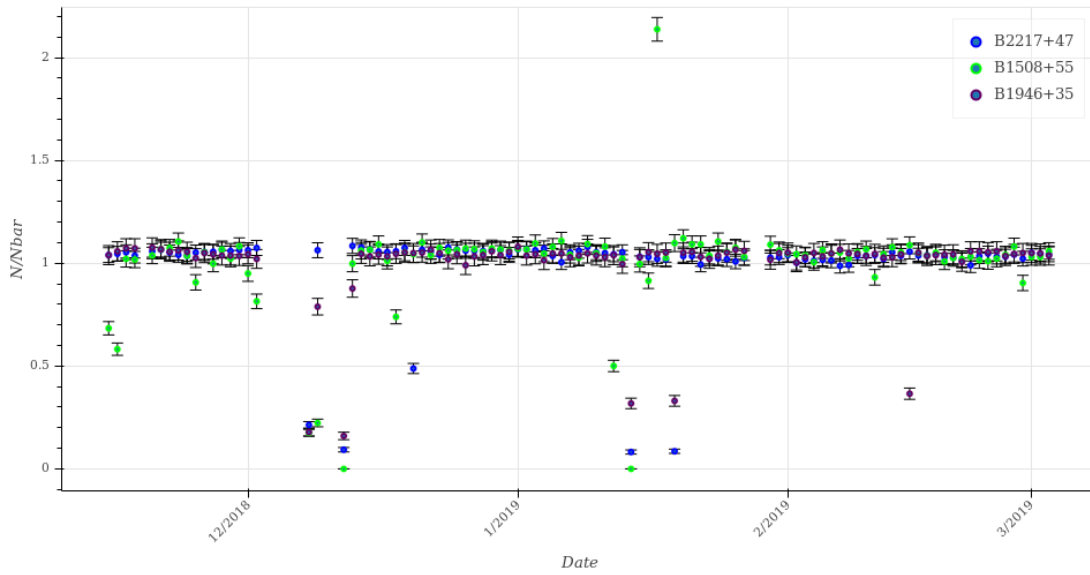
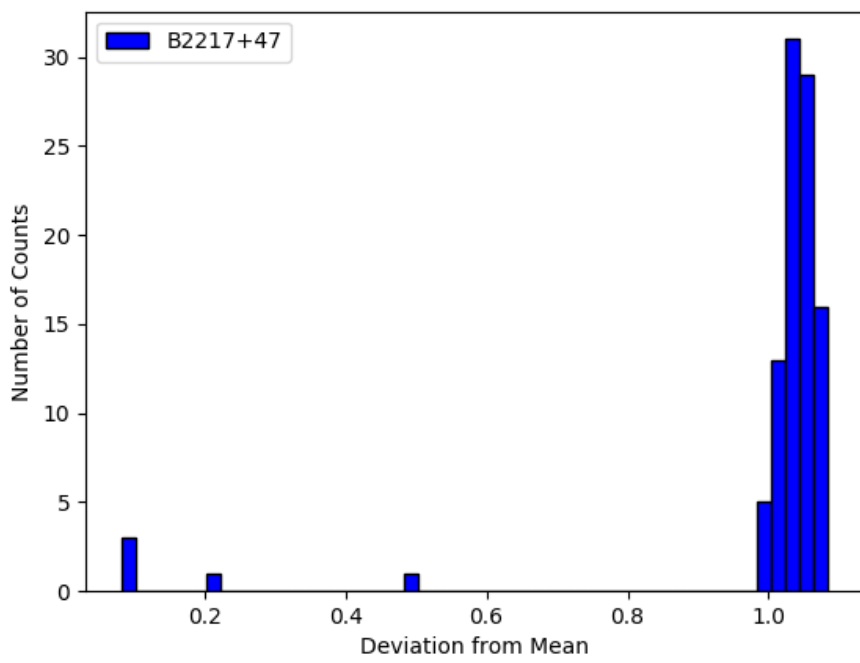
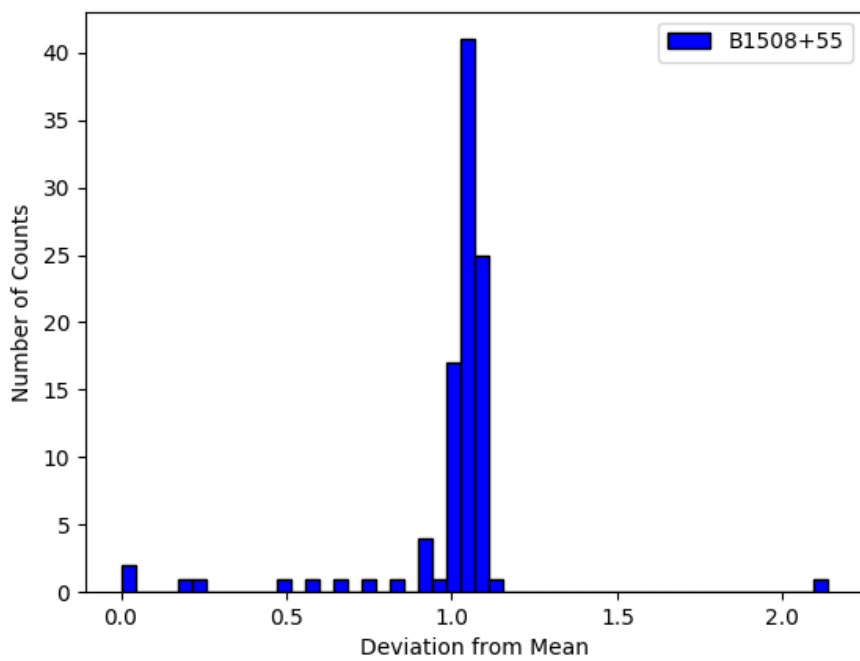
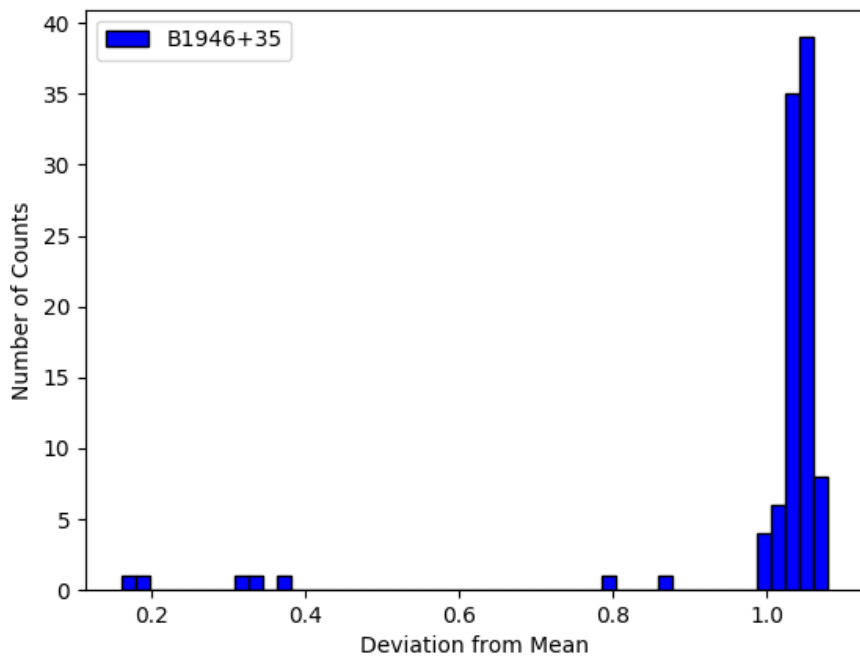


Figure 15: The pulse count per day over the mean pulse count of the three most stable sources plotted over time. In spite of a few outliers, the three are very concentrated around the mean.





A.3 Other Results of Interest

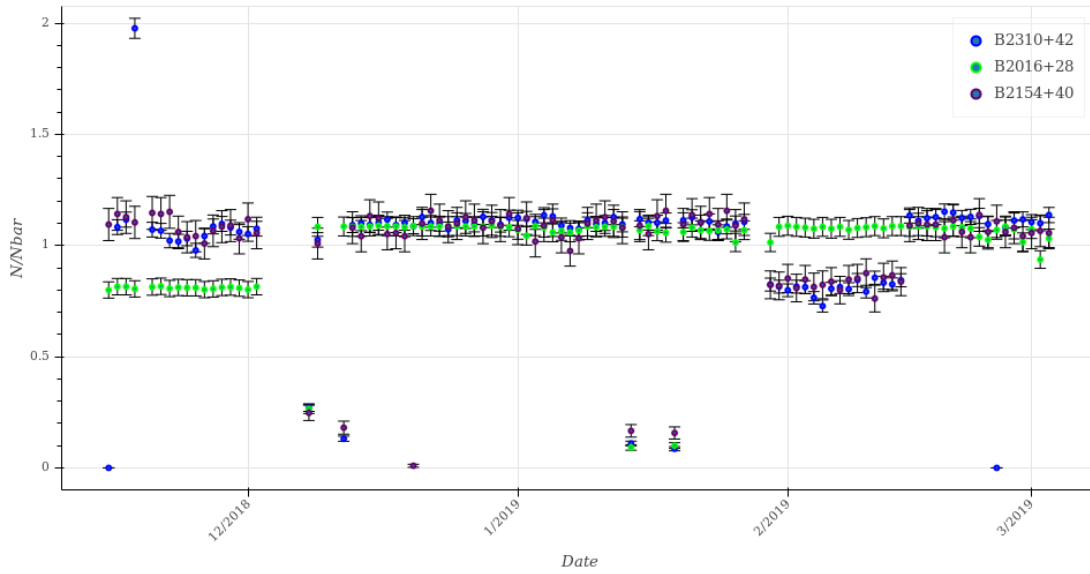


Figure 16: Notice the step in the data. These are the only three sources out of all the 193 analyzed that display this phenomenon.

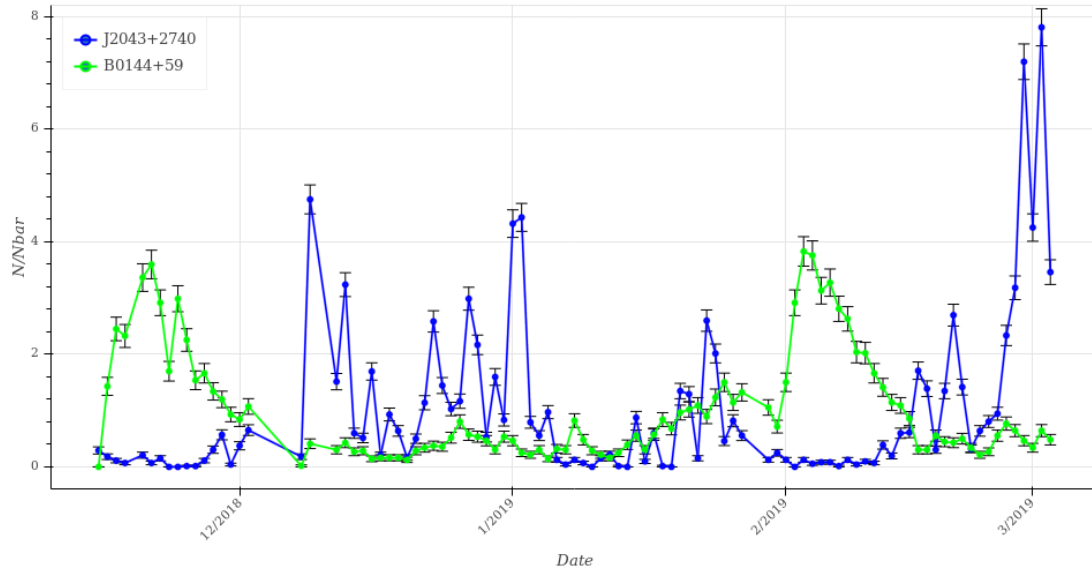


Figure 17: Notice the wild oscillation. The source in blue has a mean pulse count of 72 and the source in green has a mean pulse count of 56. They don't even make it in the top 50, with respective ranking of 55 and 61. Neither of these seem to be known for scintillation nor giant pulses

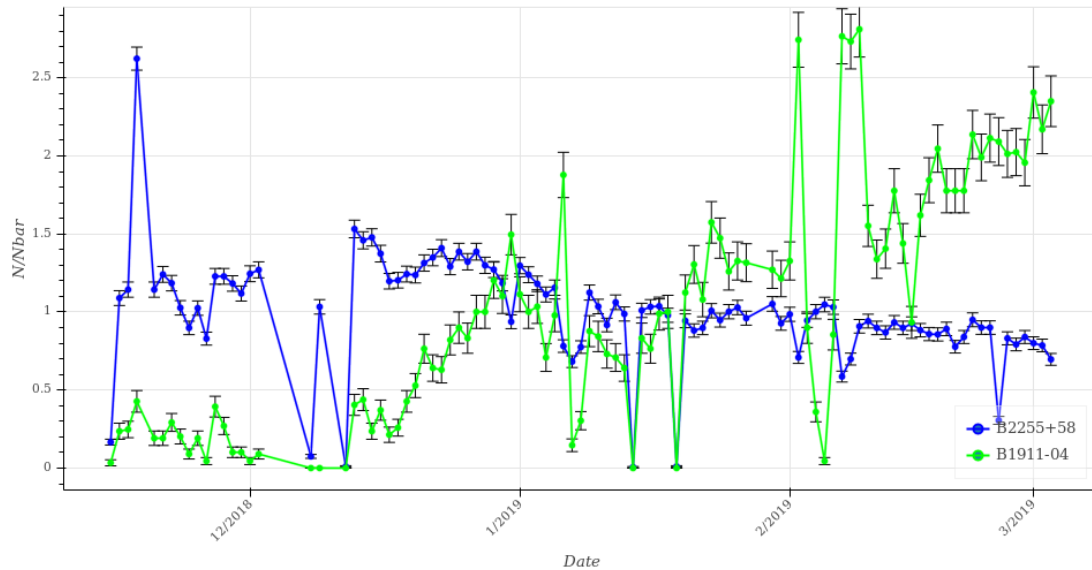


Figure 18: Notice the blue source dropping as the green source rises. The source in blue has a mean pulse count of 481, ranking it 10th and the source in green has a mean pulse count of 89 ranking it 46th. Besides general features in common such as a drop in early December, the two sources draw out an 'X'.

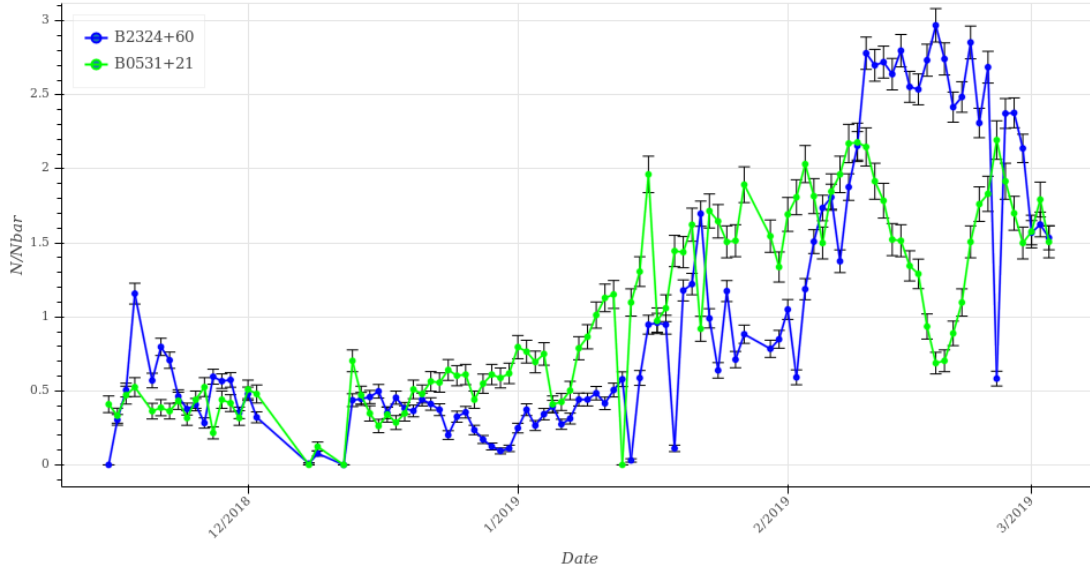


Figure 19: The two sources oscillate wildly, especially the blue source, which exhibits a very peculiar pattern. It seems almost as if its activity varies heavily over time. The mean SNR of the blue source is rather stable, while that of the green source does indeed display a big valley in mid-February. We note that the green source is the Crab pulsar, known for giant pulses, and B2324+60 is already known for scintillation. [6]

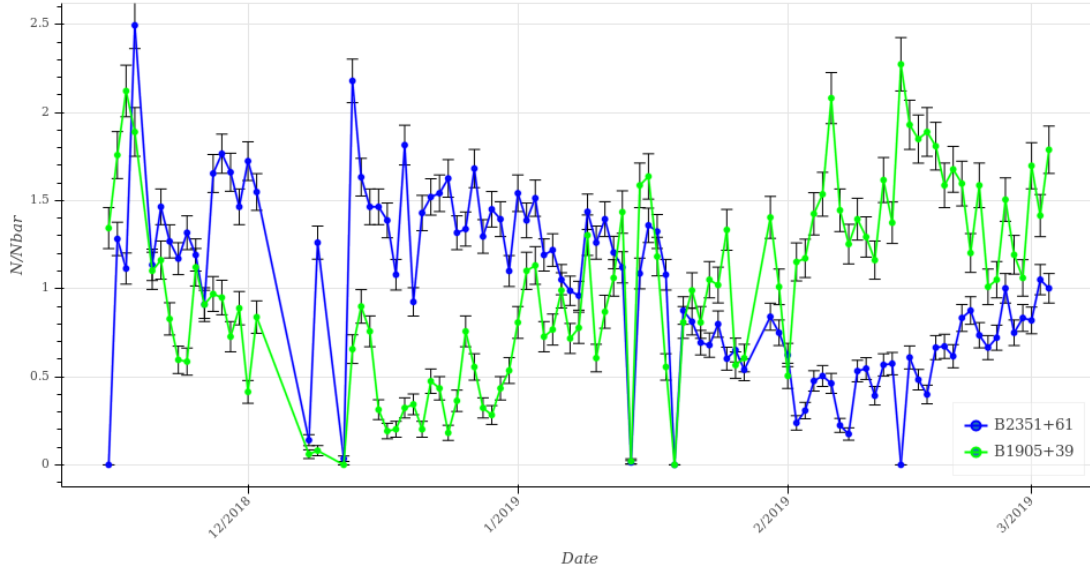


Figure 20: These two sources appear to have a sinusoidal pulse count over time. Their mean SNR also varies in a similar way, suggesting they might be magnified by some cloud rotating around them. B2351+61 is also already known for scintillation. [6] Note that there are many more sources that exhibit this behaviour!